Acta Mech. Sin. (2011) 27(6):1023–1033
DOI 10.1007/s10409-011-0509-x

RESEARCH PAPER

Geometric nonlinear dynamic analysis of curved beams using curved beam element

Ke-Qi Pan · Jin-Yang Liu

Received: 7 March 2011 / Revised: 29 April 2011 / Accepted: 7 June 2011

Abstract Instead of using the previous straight beam element to approximate the curved beam, in this paper, a curvilinear coordinate is employed to describe the deformations, and a new curved beam element is proposed to model the curved beam. Based on exact nonlinear strain-displacement relation, virtual work principle is used to derive dynamic equations for a rotating curved beam, with the effects of axial extensibility, shear deformation and rotary inertia taken into account. The constant matrices are solved numerically utilizing the Gauss quadrature integration method. Newmark and Newton–Raphson iteration methods are adopted to solve the differential equations of the rigid-flexible coupling system. The present results are compared with those obtained by commercial programs to validate the present finite method. In order to further illustrate the convergence and efficiency characteristics of the present modeling and computation formulation, comparison of the results of the present formulation with those of the ADAMS software are made. Furthermore, the present results obtained from linear formulation are compared with those from nonlinear formulation, and the special dynamic characteristics of the curved beam are concluded by comparison with those of the straight beam.

Keywords Curved beam element · Geometric nonlinear formulation · Rigid-flexible coupling

The project was supported by the National Natural Science Foundation of China (10872126) and Research Fund for the Doctoral Program of Higher Education of China (20100073110007).

K.-Q. Pan · J.-Y. Liu (✉)
School of Naval Architecture,
Ocean and Civil Engineering,
Shanghai Jiaotong University,
200240 Shanghai, China
e-mail: liujy@sjtu.edu.cn

1 Introduction

Dynamic performance of rotating flexible structures such as spacecrafts, robotics and high-speed turbine blades have been studied for a long time. A rotating system is characterized by the coupling between rotating motion and elastic deflection. The effect of the elastic deformation can significantly influence the large overall motion of the system. Particularly, with the increase of the angular velocity, the accuracy in modeling the deformation plays an important role, there are thus many studies focused on geometrically nonlinear behavior. By using an axial stretch variable, a criterion on inclusion of stiffening terms of a beam was put forward using an influence ratio [1], and then an experiment was carried out to verify the correctness of the nonlinear formulation [2]. Moreover, absolute nodal coordinate formulation [3] was developed to solve large deformation problems. On the basis of exact strain-displacement relation, Liu et al. [4] proposed a new hybrid-coordinate formulation to consider geometric nonlinear effect, such formulation is suitable for simulating flexible multi-body systems with large deformation. However, these investigations are limited to straight beams and rectangular thin plates. Few researchers have shown interest on the research of rigid-flexible dynamics of irregular shaped complex structures, such as curved beams and shells. Liu et al. [5] combined the characteristics of hybrid coordinate formulation and absolute nodal coordinate formulation to investigate the dynamics of a curved beam. Based on coupling deformation element, Liu et al. [6] established a flexible curved beam model which avoided the integral shortcomings of hybrid-coordinate formulation. Zhang et al. [7] proposed a dynamic spatial curved beam model using straight beam finite element. Sugiyama et al. [8] used the absolute nodal coordinate formulation to investigate the curved beam. Although these researches successfully modeled the curved beam, they all used the concept of straight beam element approximation for finite element discretization of the curved

beams. Owing to the straight beam element approximation, even if lots of straight beam elements are used, the accuracy of the results can not be guaranteed.

In the finite element analysis of curved structures, the use of curved beam elements based on curvilinear strain field description is an efficient alternative to the employment of large numbers of straight beam elements to approximate the true curve shape. Ganapathi et al. [9] proposed a curved cubic B-spline beam element for free vibrations and static analysis. According to thin shell theory, Raveendranath et al. [10] proposed a two-node locking free shear flexible curved beam element which can circumvent shear and membrane locking problem, subsequently, Raveendranath et al. [11] further extended it to a three-node shear-flexible curved beam element based on coupled displacement field interpolations. Friedman et al. [12] utilized the trigonometric functions as the interpolation function. Wu et al. [13] presented the curved element by a set of simple implicit interpolation function on the basis of Ref. [12], and established transformation relations between the curved beam and the straight beam elements to investigate the in plane vibration of hybrid beam. By adding the shear and torsion degree of freedom, Wu et al. [14] extended this method to solve the out-of-plane problem. Saffari et al. [15] and Yang et al. [16] presented the three-node beam element based on the curvature by the transformation matrix between nodal curvatures and nodal displacements, the final finite element equilibrium equation were written in terms of the displacement components of the two edge nodes. Leung et al. [17] presented Fourier *p*-elements for in-plane vibration of thin and thick curved beams by introducing additional internal degrees of freedom which are sine functions to Fourier trigonometric functions to avoid membrane and shear locking and to increase the convergence and stability of the curved element. Based on an identical concept, Kim et al. [18] added bubble functions to the displacement field interpolation so as to enhance substantially the numerical accuracy, especially in predicting high vibration modes. Although most of the above studies adopted the curved beam element to approximate the curved beam, they focused mainly on the free vibration and static problems, few researchers have considered the rigid-flexible coupling dynamics for curved beams. Moreover, the suitability of these curved elements for dynamic analysis was not verified, and the influences of geometrical nonlinearity of the curved beam were not included.

For the rigid-flexible coupling dynamics, Park et al. [19] investigated the dynamic characteristics of a rotating curved beam with a tip mass. It was indicated that the curved beam with moderate curvature is important for understanding the characteristic of the curved structures, however, in Ref. [19], the radius of the curvature of the curved beam is so large that the curved beam approaches a straight beam, therefore the finite element method used in this paper is not persuasive enough. Since Lagrange element formulation is much less susceptible to shear locking than the serendipity formulation, and the completely integrated cubic Lagrange element exhibits no locking, no spurious eigenvalues and rapid convergence to thin plated solution [20], one dimensional cubic Lagrange element is developed to discrete the curved beam by isoparametric formulation in this paper. The basic idea of isoparametric interpolation is to interpolate the element geometry from the coordinates of the nodes by the Lagrange element.

In this study, the curved beam with large curvature is selected for rigid-flexible coupling dynamic analysis, and the dynamic behaviors of curved beams driven by external forces are investigated. The isoparametric formulation is employed for discretization. Owing to the complexity the rational algebraic functions involved in the integrals, Gauss quadrature is introduced for calculating the constant matrix. Based on exact strain-displacement relation and using virtual work principle, equations of motion for a rotating curved beam are derived. Newmark time integration scheme associated with Newton–Raphson iteration is used to improve the efficiency. Agreement of the present results with those obtained by commercial programs verifies the correctness of the present formulation. Finally, the results for the curved beam obtained by the proposed formulation are compared with those for the straight beam to show specific rigid-flexible coupling characteristics of the curved beam.

2 The displacement field

A curved beam with constant curvature cantilevered onto a rigid hub is shown in Fig. 1, in which α is the subtended angle of the curved beam, R is the curvature radius of the curved beam, and R_{h} is the radius of the hub. The displacement fields of an arbitrary Point P at subtended angle β are given as follows

$$\bar{u}(x, y, t) = u(x, t) - y\varphi(x, t), \tag{1}$$

$$\bar{v}(x, y, t) = v(x, t), \tag{2}$$

where x is the arc length along the neutral axis from the left end and y is the distance along the thickness direction, and $\bar{u}(x, y, t)$ and $\bar{v}(x, y, t)$ are the tangential and transverse elastic deformation, respectively, and φ represents the rotation angle of the cross section.

The nonlinear longitudinal and shear strain are defined, respectively, as [19]

$$\varepsilon_x = \left(\frac{\mathrm{d}u}{\mathrm{d}x} - \frac{v}{R}\right) + \frac{1}{2}\left[\left(\frac{\mathrm{d}u}{\mathrm{d}x}\right)^2 + \left(\frac{\mathrm{d}v}{\mathrm{d}x}\right)^2\right] - y\frac{\mathrm{d}\varphi}{\mathrm{d}x}, \tag{3}$$

$$\gamma_{xy} = \frac{\mathrm{d}v}{\mathrm{d}x} + \frac{u}{R} - \varphi. \tag{4}$$

In Eq. (3), the terms in the first and the second bracket are the linear and the nonlinear strains, respectively. Especially, the nonlinear term $\frac{1}{2}\left(\frac{\mathrm{d}u}{\mathrm{d}x}\right)^2$ arising from the longitudinal stretching is taken into account in this paper, which is always ig-

nored in the previous studies on dynamics of straight beam system. Since the longitudinal deformation of the straight beams is small, such term can be neglected in the equations of motion for straight beam systems. However, the longitudinal deformation of curved beams is larger compared with straight beams, therefore, the negligence of such term may lead to simulation error in case that the quadratic term of the gradient of the longitudinal deformation approaches the quadratic term of the gradient of the transverse deformation.

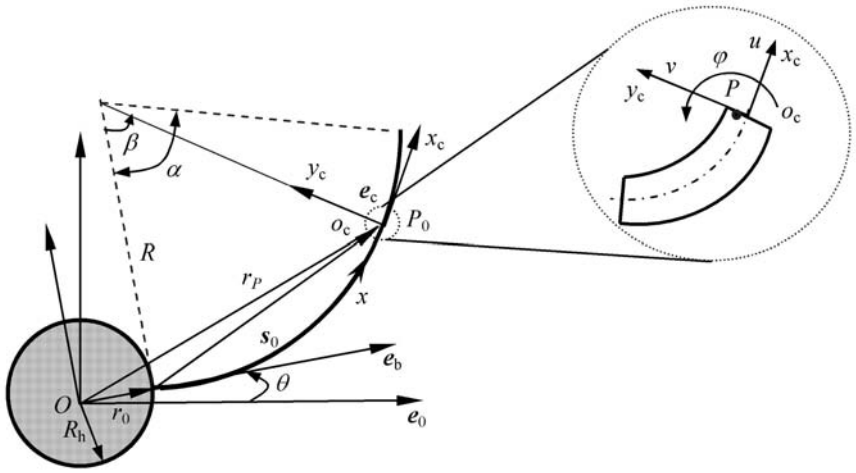

Fig. 1 Configure of a rotating curved beam

The stress–strain relations of the curved beam including shear effects are given by

$$\sigma_x = E\varepsilon_x, \qquad \tau_{xy} = G\gamma_{xy}, \tag{5}$$

where E is the modulus of elasticity and G is the shear modulus.

The virtual work of the elastic force can be written as

$$\delta W_e = -A\Big(\int_0^L \delta\varepsilon_x E\varepsilon_x \mathrm{d}x + \int_0^L k\delta\gamma_{xy} G\gamma_{xy} \mathrm{d}x \Big), \tag{6}$$

where k denotes the shear correction factor.

3 The kinematics description of the curved beam

The kinematics relations of an arbitrary point on the beam are described with the aid of three coordinate systems as shown in Fig. 1: an inertial frame $\boldsymbol{e}_0$ located at O, a hub body-fixed rotating frame $\boldsymbol{e}_b$ and a local curvilinear frame $\boldsymbol{e}_c(o_c x_c y_c)$ fixed on an arbitrary Point P_0 of the neutral axis of the curved beam, with $o_c x_c$ along the tangent of the neutral axis, and $o_c y_c$ along the normal vector, which is directed to the center of the arc of the beam.

The coordinate matrix of the displacement of an arbitrary point with respect to $\boldsymbol{e}_0$ can be written as

$$\boldsymbol{r} = \boldsymbol{A}_\theta(\boldsymbol{r}_0' + \boldsymbol{s}_0' + \boldsymbol{A}_\beta\boldsymbol{\rho}_0' + \boldsymbol{A}_\beta\boldsymbol{u}'), \tag{7}$$

where $\boldsymbol{r}_0' = [R_h \;\; 0]^T$ represents the coordinate matrix of $\boldsymbol{r}_0$ defined in $\boldsymbol{e}_0$, $\boldsymbol{s}_0' = [X \;\; Y]^T$ represent the coordinates of $\boldsymbol{s}_0$ defined in $\boldsymbol{e}_b$, $\boldsymbol{\rho}_0' = [0 \;\; y]^T$ is the transverse coordinate matrix of arbitrary point P on the cross section and $\boldsymbol{u}' = [\overline{u} \;\; \overline{v}]^T$ represent the coordinate matrix of deformation displacement of Point P which is also defined in frame $\boldsymbol{e}_c$. $\boldsymbol{A}_\theta$ represents the transformation matrix of frame $\boldsymbol{e}_b$ with respect to frame $\boldsymbol{e}_0$, and $\boldsymbol{A}_\beta$ represents the transformation matrix of frame $\boldsymbol{e}_c$ with respect to frame $\boldsymbol{e}_b$, which are, respectively, given by

$$\boldsymbol{A}_\theta = \begin{bmatrix} \cos\theta & -\sin\theta \\ \sin\theta & \cos\theta \end{bmatrix}, \quad \boldsymbol{A}_\beta = \begin{bmatrix} \cos\beta & -\sin\beta \\ \sin\beta & \cos\beta \end{bmatrix}. \tag{8}$$

Differentiation of Eq. (7) leads to

$$\dot{\boldsymbol{r}} = \tilde{\boldsymbol{I}}\boldsymbol{A}_\theta\dot{\theta}(\boldsymbol{r}_0' + \boldsymbol{s}_0' + \boldsymbol{A}_\beta\boldsymbol{\rho}_0' + \boldsymbol{A}_\beta\boldsymbol{u}') + \boldsymbol{A}_\theta\boldsymbol{A}_\beta\dot{\boldsymbol{u}}', \tag{9}$$

and the second differentiation of Eq. (7) leads to

$$\begin{aligned} \ddot{\boldsymbol{r}} = & -\boldsymbol{A}_\theta\dot{\theta}^2(\boldsymbol{r}_0' + \boldsymbol{s}_0' + \boldsymbol{A}_\beta\boldsymbol{\rho}_0' + \boldsymbol{A}_\beta\boldsymbol{u}') \\ & +\tilde{\boldsymbol{I}}\boldsymbol{A}_\theta\ddot{\theta}(\boldsymbol{r}_0' + \boldsymbol{s}_0' + \boldsymbol{A}_\beta\boldsymbol{\rho}_0' + \boldsymbol{A}_\beta\boldsymbol{u}') \\ & +2\tilde{\boldsymbol{I}}\boldsymbol{A}_\theta\dot{\theta}\boldsymbol{A}_\beta\dot{\boldsymbol{u}}' + \boldsymbol{A}_\theta\boldsymbol{A}_\beta\ddot{\boldsymbol{u}}', \end{aligned} \tag{10}$$

where $\tilde{\boldsymbol{I}}$ represents a skew-symmetric matrix and can be written as $\tilde{\boldsymbol{I}} = \begin{bmatrix} 0 & -1 \\ 1 & 0 \end{bmatrix}$.

The virtual displacement coordinate vector reads

$$\delta\boldsymbol{r} = \tilde{\boldsymbol{I}}\boldsymbol{A}_\theta\delta\theta(\boldsymbol{r}_0' + \boldsymbol{s}_0' + \boldsymbol{A}_\beta\boldsymbol{\rho}_0' + \boldsymbol{A}_\beta\boldsymbol{u}') + \boldsymbol{A}_\theta\boldsymbol{A}_\beta\delta\boldsymbol{u}'. \tag{11}$$

4 Lagrange elements and isoparametric formulation

4.1 One dimensional Lagrange elements

The shape function N_i of a Lagrange element with n nodes

coincides with a $(n-1)$-th Lagrange polynomial, which is given by

$$N_i(X) = \prod_{j=1, j\neq i}^{n} \frac{X - X_j}{X_i - X_j}, \qquad i = 1, 2, \cdots, n, \tag{12}$$

where $X_1, X_2, \cdots, X_n$ are the coordinates of node points, n is the total number of nodes of the curved beam element.

A dimensionless natural coordinate ξ is introduced as

$$\xi = \frac{2(X - X_c)}{l_e}, \tag{13}$$

where X_c is the Cartesian coordinate of the element midpoint and l_e is the length of the element.

After substituting Eq. (13) into Eq. (12), the shape functions can be written in terms of the natural coordinate as

$$\bar{N}_i(\xi) = \prod_{j=1, j\neq i}^{n} \frac{\xi - \xi_j}{\xi_i - \xi_j}, \quad i = 1, 2, \cdots, n, \qquad -1 \le \xi \le 1. \tag{14}$$

4.2 The parametric interpolation of the element geometry and elastic deformation

The Cartesian coordinates of the initial configure of axis line of curved beam element, can be defined as

$$X(\xi) = \sum_{i=1}^{n} \bar{N}_i X_i^e, \qquad Y(\xi) = \sum_{i=1}^{n} \bar{N}_i Y_i^e, \tag{15}$$

where (X_i^e, Y_i^e) is the nodes coordinate defined in frame $\boldsymbol{e}_b$. In this paper, a cubic Lagrange element with four nodes ($n = 4$) is selected, as shown in Fig. 2b.

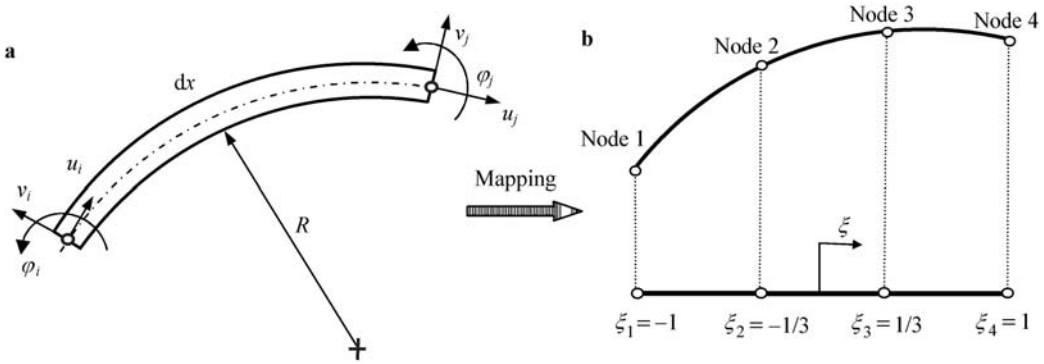

Fig. 2 Elements transformation by isoparametric formulation. **a** Part of the curved beam; **b** Natural coordinate system ξ and 4-noded element

According to Eq. (15), the infinitesimal arc element dx can be mapped into natural coordinated system, which can be expressed as

$$\mathrm{d}x = J_e(\xi)\mathrm{d}\xi, \tag{16}$$

where $J_e(\xi) = \sqrt{(\mathrm{d}X/\mathrm{d}\xi)^2 + (\mathrm{d}Y/\mathrm{d}\xi)^2}$.

Elastic deformations and rotational angle of the cross section are interpolated as

$$\begin{aligned} u(\xi, t) &= \sum_{i=1}^{4} \bar{N}_i(\xi) u_i(t), \\ v(\xi, t) &= \sum_{i=1}^{4} \bar{N}_i(\xi) v_i(t), \\ \varphi(\xi, t) &= \sum_{i=1}^{4} \bar{N}_i(\xi) \varphi_i(t). \end{aligned} \tag{17}$$

From Eqs. (16) and (17), the Cartesian derivatives of the elastic deformation can be expressed as

$$\frac{\mathrm{d}u}{\mathrm{d}x} = \frac{\mathrm{d}u}{\mathrm{d}\xi}\frac{\mathrm{d}\xi}{\mathrm{d}x} = \frac{1}{J_e}\sum_{i=1}^{4} \frac{\mathrm{d}\bar{N}_i}{\mathrm{d}\xi} u_i, \tag{18}$$

$$\frac{\mathrm{d}v}{\mathrm{d}x} = \frac{\mathrm{d}v}{\mathrm{d}\xi}\frac{\mathrm{d}\xi}{\mathrm{d}x} = \frac{1}{J_e}\sum_{i=1}^{4} \frac{\mathrm{d}\bar{N}_i}{\mathrm{d}\xi} v_i, \tag{19}$$

$$\frac{\mathrm{d}\varphi}{\mathrm{d}x} = \frac{\mathrm{d}\varphi}{\mathrm{d}\xi}\frac{\mathrm{d}\xi}{\mathrm{d}x} = \frac{1}{J_e}\sum_{i=1}^{4} \frac{\mathrm{d}\bar{N}_i}{\mathrm{d}\xi} \varphi_i. \tag{20}$$

The displacement can be rewritten as

$$u = \boldsymbol{N}_1(\xi)\boldsymbol{p}_e, \quad v = \boldsymbol{N}_2(\xi)\boldsymbol{p}_e, \quad \varphi = \boldsymbol{N}_3(\xi)\boldsymbol{p}_e, \tag{21}$$

where matrix $\boldsymbol{N}_i(\xi)$ is the shape function, which reads

$$\boldsymbol{N}_1(\xi) = [\,\bar{N}_1(\xi) \;\; 0 \;\; 0 \;\; \bar{N}_2(\xi) \;\; 0 \;\; 0 \;\; \bar{N}_3(\xi) \;\; 0 \;\; 0 \;\; \bar{N}_4(\xi) \;\; 0 \;\; 0\,], \tag{22}$$

$$\boldsymbol{N}_2(\xi) = [\,0 \;\; \bar{N}_1(\xi) \;\; 0 \;\; 0 \;\; \bar{N}_2(\xi) \;\; 0 \;\; 0 \;\; \bar{N}_3(\xi) \;\; 0 \;\; 0 \;\; \bar{N}_4(\xi) \;\; 0\,], \tag{23}$$

$$\boldsymbol{N}_3(\xi) = [\,0 \;\; 0 \;\; \bar{N}_1(\xi) \;\; 0 \;\; 0 \;\; \bar{N}_2(\xi) \;\; 0 \;\; 0 \;\; \bar{N}_3(\xi) \;\; 0 \;\; 0 \;\; \bar{N}_4(\xi)\,], \tag{24}$$

and $\boldsymbol{p}_e = [\,u_1 \quad v_1 \quad \varphi_1 \quad \cdots \quad u_n \quad v_n \quad \varphi_n\,]^{\mathrm{T}}$ is the time-dependent vector of generalized coordinate of a curved beam element. Substituting Eqs. (21)–(24) into Eqs. (1) and (2), one obtains that

$$\bar{u}(x,y,t) = \boldsymbol{N}_1\boldsymbol{p}_e - y\boldsymbol{N}_3\boldsymbol{p}_e, \tag{25}$$

$$\bar{v}(x,y,t) = \boldsymbol{N}_2\boldsymbol{p}_e. \tag{26}$$

For the convenience of expression, let $\boldsymbol{p}$ denote the global nodal coordinate vector, and $\boldsymbol{B}_e$ denote the element Boolean matrix, the relation between $\boldsymbol{p}_e$ and $\boldsymbol{p}$ are given by $\boldsymbol{p}_e = \boldsymbol{B}_e\boldsymbol{p}$. Then, Eqs. (1) and (2) can be written as

$$\boldsymbol{u}' = \begin{bmatrix} \bar{u} \\ \bar{v} \end{bmatrix} = \boldsymbol{S}\boldsymbol{p}, \tag{27}$$

where

$$\boldsymbol{S} = \begin{bmatrix} \boldsymbol{N}_1 \\ \boldsymbol{N}_2 \end{bmatrix}\boldsymbol{B}_e - y\begin{bmatrix} \boldsymbol{N}_3 \\ \boldsymbol{0} \end{bmatrix}\boldsymbol{B}_e. \tag{28}$$

5 Equations of motion

The virtual work of the inertial force is defined as

$$\delta W_i = -\rho\int_V \delta\boldsymbol{r}^{\mathrm{T}}\ddot{\boldsymbol{r}}\mathrm{d}V - \delta\theta\, J_h\ddot{\theta}, \tag{29}$$

where V represents the volume of the curved beam, and ρ is the mass density of the beam, and J_h is the moment of inertia of the hub.

Substituting Eqs. (10), (11) and (27) into Eq. (29), one obtains

$$\delta W_i = -\delta\boldsymbol{q}^{\mathrm{T}}\boldsymbol{M}\ddot{\boldsymbol{q}} + \delta\boldsymbol{q}^{\mathrm{T}}\boldsymbol{Q}_m, \tag{30}$$

where $\boldsymbol{q} = [\,\theta \quad \boldsymbol{p}\,]^{\mathrm{T}}$ is the generalized coordinate of system, and the generalized mass and inertia force matrices take the form of

$$\boldsymbol{M} = \begin{bmatrix} M_{\theta\theta} & \boldsymbol{M}_{\theta p} \\ \boldsymbol{M}_{p\theta} & \boldsymbol{M}_{pp} \end{bmatrix}, \qquad \boldsymbol{Q}_m = \begin{bmatrix} Q_\theta \\ \boldsymbol{Q}_p \end{bmatrix}, \tag{31}$$

where

$$M_{\theta\theta} = J_h + \rho I\alpha R + \sum_{e=1}^{N_e}\int_{-1}^{1}\rho A(\boldsymbol{r}_0' + \boldsymbol{s}_0' + \boldsymbol{A}_\beta\boldsymbol{S}\boldsymbol{p})^{\mathrm{T}} \times(\boldsymbol{r}_0' + \boldsymbol{s}_0' + \boldsymbol{A}_\beta\boldsymbol{S}\boldsymbol{p})J_e\mathrm{d}\xi, \tag{32}$$

$$\boldsymbol{M}_{\theta p} = \sum_{e=1}^{N_e}\Big[\int_{-1}^{1}\rho A(\boldsymbol{r}_0' + \boldsymbol{s}_0' + \boldsymbol{A}_\beta\boldsymbol{S}\boldsymbol{p})^{\mathrm{T}}\boldsymbol{A}_\theta^{\mathrm{T}}\tilde{\boldsymbol{I}}^{\mathrm{T}} \times\boldsymbol{A}_\theta\boldsymbol{A}_\beta\boldsymbol{S}\,J_e\mathrm{d}\xi + \int_{-1}^{1}\rho I\boldsymbol{N}_3 J_e\mathrm{d}\xi\boldsymbol{B}_e\Big], \tag{33}$$

$$\boldsymbol{M}_{p\theta} = \boldsymbol{M}_{\theta p}^{\mathrm{T}}, \qquad \boldsymbol{M}_{pp} = \sum_{e=1}^{N_e}\int_{-1}^{1}\rho A\boldsymbol{S}^{\mathrm{T}}\boldsymbol{S}\,J_e\mathrm{d}\xi, \tag{34}$$

$$Q_\theta = -2\,\dot{\theta}\sum_{e=1}^{N_e}\int_{-1}^{1}\rho A(\boldsymbol{r}_0' + \boldsymbol{s}_0' + \boldsymbol{A}_\beta\boldsymbol{S}\boldsymbol{p})^{\mathrm{T}} \times\boldsymbol{A}_\beta\boldsymbol{S}\dot{\boldsymbol{p}}\,J_e\mathrm{d}\xi, \tag{35}$$

$$\boldsymbol{Q}_p = \sum_{e=1}^{N_e}\int_{-1}^{1}\rho A(\boldsymbol{S}^{\mathrm{T}}\boldsymbol{A}_\beta^{\mathrm{T}}) \times[\dot{\theta}^2(\boldsymbol{r}_0' + \boldsymbol{s}_0' + \boldsymbol{A}_\beta\boldsymbol{S}\boldsymbol{p}) - 2\tilde{\boldsymbol{I}}\dot{\theta}\boldsymbol{A}_\beta\boldsymbol{S}\dot{\boldsymbol{p}}]J_e\mathrm{d}\xi, \tag{36}$$

where A is the area of the cross section and N_e is the number of elements.

Considering Eqs. (11) and (27), the virtual work of the other external forces can be written as

$$\delta W_{\mathrm{F}} = \int_V \delta\boldsymbol{r}^{\mathrm{T}}\boldsymbol{f}\,\mathrm{d}V + \delta\theta T = \delta\boldsymbol{q}^{\mathrm{T}}\boldsymbol{Q}_{\mathrm{F}}, \tag{37}$$

where $\boldsymbol{f}$ represents the gravitational force vector defined in the inertial frame, and T represents the external moment applied on the hub, respectively. The generalized external force $\boldsymbol{Q}_{\mathrm{F}}$ is given by

$$\boldsymbol{Q}_{\mathrm{F}} = \begin{bmatrix} A\sum_{e=1}^{N_e}\int_{-1}^{1}(\boldsymbol{r}_0' + \boldsymbol{s}_0' + \boldsymbol{A}_\beta\boldsymbol{S}\boldsymbol{p})^{\mathrm{T}}\boldsymbol{A}_\theta^{\mathrm{T}}\tilde{\boldsymbol{I}}^{\mathrm{T}}\boldsymbol{f}\,J_e\mathrm{d}\xi + T \\ A\sum_{e=1}^{N_e}\int_{-1}^{1}\boldsymbol{S}^{\mathrm{T}}\boldsymbol{A}_\beta^{\mathrm{T}}\boldsymbol{A}_\theta^{\mathrm{T}}\boldsymbol{f}\,J_e\mathrm{d}\xi \end{bmatrix}. \tag{38}$$

By substituting Eqs. (3), (4) , (27) and (28) into Eq. (6), the virtual work of the internal force considering geometric nonlinear effect can be written as

$$\delta W_e = \delta\boldsymbol{q}^{\mathrm{T}}\boldsymbol{Q}_e = -\delta\boldsymbol{p}^{\mathrm{T}}[\boldsymbol{K}_e + \boldsymbol{K}_n(\boldsymbol{p}_e)]\boldsymbol{p}, \tag{39}$$

where $\boldsymbol{K}_e$ is the constant stiffness matrix and $\boldsymbol{K}_n(\boldsymbol{p}_e)$ is the time-variant nonlinear stiffness matrix, which are given by

$$\boldsymbol{K}_e = \sum_{e=1}^{N_e}\boldsymbol{B}_e^{\mathrm{T}}\Big\{\int_{-1}^{1}\Big[EA\Big(\boldsymbol{D}_{e1}^{\mathrm{T}}\boldsymbol{D}_{e1} - \frac{1}{R}\boldsymbol{D}_{e1}^{\mathrm{T}}\boldsymbol{N}_2 - \frac{1}{R}\boldsymbol{N}_2^{\mathrm{T}}\boldsymbol{D}_{e1} + \frac{1}{R^2}\boldsymbol{N}_2^{\mathrm{T}}\boldsymbol{N}_2\Big) + EI\boldsymbol{D}_{e3}^{\mathrm{T}}\boldsymbol{D}_{e3} + GkA\Big(\boldsymbol{D}_{e2} + \frac{1}{R}\boldsymbol{N}_1 - \boldsymbol{N}_3\Big)^{\mathrm{T}} \times\Big(\boldsymbol{D}_{e2} + \frac{1}{R}\boldsymbol{N}_1 - \boldsymbol{N}_3\Big)\Big]J_e\mathrm{d}\xi\Big\}\boldsymbol{B}_e, \tag{40}$$

$$\boldsymbol{K}_n(\boldsymbol{p}_e) = \sum_{e=1}^{N_e}\boldsymbol{B}_e^{\mathrm{T}}\Big\{EA\int_{-1}^{1}[(\boldsymbol{D}_{e1}^{\mathrm{T}} - \boldsymbol{N}_2^{\mathrm{T}}/R)\boldsymbol{p}_e^{\mathrm{T}} \times(\boldsymbol{D}_{e1}^{\mathrm{T}}\boldsymbol{D}_{e1} + \boldsymbol{D}_{e2}^{\mathrm{T}}\boldsymbol{D}_{e2})/2 + (\boldsymbol{D}_{e1}^{\mathrm{T}} - \boldsymbol{N}_2^{\mathrm{T}}/R)\boldsymbol{p}_e \times(\boldsymbol{D}_{e1}^{\mathrm{T}}\boldsymbol{D}_{e1} + \boldsymbol{D}_{e2}^{\mathrm{T}}\boldsymbol{D}_{e2}) + \boldsymbol{p}_e^{\mathrm{T}}(\boldsymbol{D}_{e1}^{\mathrm{T}}\boldsymbol{D}_{e1} + \boldsymbol{D}_{e2}^{\mathrm{T}}\boldsymbol{D}_{e2}) \times\boldsymbol{p}_e(\boldsymbol{D}_{e1}^{\mathrm{T}}\boldsymbol{D}_{e1} + \boldsymbol{D}_{e2}^{\mathrm{T}}\boldsymbol{D}_{e2})/2]J_e\mathrm{d}\xi\Big\}\boldsymbol{B}_e, \tag{41}$$

where $\boldsymbol{D}_{ei} = \mathrm{d}\bar{\boldsymbol{N}}_i/(J_e\mathrm{d}\xi)$, $i = 1, 2, 3$. The time-variant nonlinear stiffness $\boldsymbol{K}_n(\boldsymbol{p}_e)$ is highly nonlinear and updated in each integration, for which, matrix separation method proposed in Ref. [4] is employed to improve the efficiency.

The elastic forces take the forms of

$$\boldsymbol{Q}_e = \begin{bmatrix} 0 \\ -[\boldsymbol{K}_e + \boldsymbol{K}_n(\boldsymbol{p}_e)]\boldsymbol{p} \end{bmatrix}. \quad (42)$$

Considering Eqs. (30), (37) and (38), application of the variation principle leads to the following variational equations

$$\delta W_i + \delta W_{\mathrm{F}} + \delta W_e = \delta \boldsymbol{q}^{\mathrm{T}}(-\boldsymbol{M}\ddot{\boldsymbol{q}} + \boldsymbol{Q}_{\mathrm{m}} + \boldsymbol{Q}_{\mathrm{F}} + \boldsymbol{Q}_e) = 0. \quad (43)$$

Suppose the independent coordinate matrix of system is $\bar{\boldsymbol{q}} = \begin{bmatrix} \theta & \bar{\boldsymbol{p}} \end{bmatrix}$. Considering the constraint conditions, the relationship between the independent and dependent coordinate matrix can be written as

$$\boldsymbol{q} = \boldsymbol{D}\bar{\boldsymbol{q}}, \quad (44)$$

where $\boldsymbol{D}$ represents the transformation matrix to satisfy the boundary condition of the beam.

According to Eq. (43), the equations of motion of the system can be obtained as

$$\bar{\boldsymbol{M}}\ddot{\bar{\boldsymbol{q}}} + \bar{\boldsymbol{K}}\bar{\boldsymbol{q}} = \bar{\boldsymbol{Q}}, \quad (45)$$

where

$$\bar{\boldsymbol{M}} = \boldsymbol{D}^{\mathrm{T}}\boldsymbol{M}\boldsymbol{D}, \qquad \bar{\boldsymbol{Q}} = \boldsymbol{D}^{\mathrm{T}}(\boldsymbol{Q}_{\mathrm{m}} + \boldsymbol{Q}_{\mathrm{F}}),$$

$$\bar{\boldsymbol{K}} = \boldsymbol{D}^{\mathrm{T}}\begin{bmatrix} 0 & \boldsymbol{0} \\ \boldsymbol{0} & \boldsymbol{K}_e + \boldsymbol{K}_n(\boldsymbol{p}_e) \end{bmatrix}\boldsymbol{D}.$$

6 Numerical method for solving differential equations

In this paper, differential equation of (45) will be solved numerically by using Newmark time stepping scheme with Newton–Raphson iteration method.

The nonlinear equations of motion at time $t + \Delta t$ are given by

$$\bar{\boldsymbol{M}}(\bar{\boldsymbol{q}}_{t+\Delta t})\ddot{\bar{\boldsymbol{q}}}_{t+\Delta t} + \bar{\boldsymbol{K}}(\bar{\boldsymbol{q}}_{t+\Delta t})\bar{\boldsymbol{q}}_{t+\Delta t} = \bar{\boldsymbol{Q}}_{t+\Delta t}(\boldsymbol{q}_{t+\Delta t}, \dot{\boldsymbol{q}}_{t+\Delta t}). \quad (46)$$

By using Newmark algorithm, the relation among velocity $\dot{\bar{\boldsymbol{q}}}_{t+\Delta t}$, acceleration $\ddot{\bar{\boldsymbol{q}}}_{t+\Delta t}$ and displacement vector $\bar{\boldsymbol{q}}_{t+\Delta t}$ is given by

$$\dot{\bar{\boldsymbol{q}}}_{t+\Delta t} = \dot{\bar{\boldsymbol{q}}}_t + \left(1 - \frac{\hat{\beta}}{2\lambda}\right)\Delta t\ddot{\bar{\boldsymbol{q}}}_t + \frac{\hat{\beta}}{\lambda\Delta t}(\bar{\boldsymbol{q}}_{t+\Delta t} - \bar{\boldsymbol{q}}_t - \dot{\bar{\boldsymbol{q}}}_t\Delta t), \quad (47)$$

$$\ddot{\bar{\boldsymbol{q}}}_{t+\Delta t} = \frac{1}{\lambda\Delta t^2}(\bar{\boldsymbol{q}}_{t+\Delta t} - \bar{\boldsymbol{q}}_t) - \frac{1}{\lambda\Delta t}\dot{\bar{\boldsymbol{q}}}_t - \left(\frac{1}{2\lambda} - 1\right)\ddot{\bar{\boldsymbol{q}}}_t, \quad (48)$$

where Δt is the time step, λ and $\hat{\beta}$ are the integration parameters, respectively.

Substituting Eqs. (47) and (48) into Eq. (46) leads to

$$\boldsymbol{\Phi} = \tilde{\boldsymbol{K}}(\bar{\boldsymbol{q}}_{t+\Delta t})\bar{\boldsymbol{q}}_{t+\Delta t} - \tilde{\boldsymbol{F}}(\bar{\boldsymbol{q}}_{t+\Delta t}) = \boldsymbol{0}, \quad (49)$$

where

$$\tilde{\boldsymbol{K}}(\bar{\boldsymbol{q}}_{t+\Delta t}) = \bar{\boldsymbol{K}}(\bar{\boldsymbol{q}}_{t+\Delta t}) + \left(\frac{1}{\lambda\Delta t^2}\right)\bar{\boldsymbol{M}}(\bar{\boldsymbol{q}}_{t+\Delta t}), \quad (50)$$

$$\tilde{\boldsymbol{F}}(\bar{\boldsymbol{q}}_{t+\Delta t}) = \bar{\boldsymbol{Q}}(\bar{\boldsymbol{q}}_{t+\Delta t}) + \bar{\boldsymbol{M}}(\bar{\boldsymbol{q}}_{t+\Delta t})$$

$$\times\left[\frac{1}{\lambda\Delta t^2}\bar{\boldsymbol{q}}_t + \frac{1}{\lambda\Delta t}\dot{\bar{\boldsymbol{q}}}_t + \left(\frac{1}{2\lambda} - 1\right)\ddot{\bar{\boldsymbol{q}}}_t\right]. \quad (51)$$

Equations (50) and (51) show that $\tilde{\boldsymbol{K}}$, $\tilde{\boldsymbol{F}}$ are functions of $\bar{\boldsymbol{q}}_{t+\Delta t}$, therefore Eq. (49) are highly nonlinear algebraic equations. Newton–Raphson iterations are adopted to improve the accuracy of the solution. The iteration process can be outlined as follows

(1) Defining $\bar{\boldsymbol{q}}^*_{t+\Delta t}$ as an accurate solution of Eq. (49), and $\boldsymbol{q}^{(i)}_{t+\Delta t}$as an approximate solution of $\bar{\boldsymbol{q}}^*_{t+\Delta t}$, expanding Eq. (49) at $\bar{\boldsymbol{q}}^{(i)}_{t+\Delta t}$ in a truncated Taylor Series

$$\boldsymbol{\Phi}(\bar{\boldsymbol{q}}_{t+\Delta t}) = \boldsymbol{\Phi}(\bar{\boldsymbol{q}}^{(i)}_{t+\Delta t}) + \boldsymbol{\Phi}_{q_{t+\Delta t}}(\bar{\boldsymbol{q}}_{t+\Delta t} - \bar{\boldsymbol{q}}^{(i)}_{t+\Delta t}), \quad (52)$$

where $\boldsymbol{\Phi}_{\boldsymbol{q}_{t+\Delta t}} = \partial\boldsymbol{\Phi}/\partial\bar{\boldsymbol{q}}_{t+\Delta t}$ is the Jacobian matrix, for which, the calculation process is most critical and most complicated, especially for the rigid-flexible coupling problem. In Eq. (52), i represents the iteration number.

(2) Defining $\bar{\boldsymbol{q}}^{(i+1)}_{t+\Delta t}$ as a modified approximate solution in the $(i+1)$-th iteration, the correction solution $\Delta\bar{\boldsymbol{q}}^{(i)}_{t+\Delta t} = \bar{\boldsymbol{q}}^{(i+1)}_{t+\Delta t} - \bar{\boldsymbol{q}}^{(i)}_{t+\Delta t}$ are calculated as

$$\Delta\bar{\boldsymbol{q}}^{(i)}_{t+\Delta t} = [\boldsymbol{\Phi}_{q_{t+\Delta t}}(\bar{\boldsymbol{q}}^{(i)}_{t+\Delta t})]^{-1}[-\boldsymbol{\Phi}(\bar{\boldsymbol{q}}^{(i)}_{t+\Delta t})]. \quad (53)$$

Then, the modified approximate solution $\bar{\boldsymbol{q}}^{(i+1)}_{t+\Delta t}$ can be obtained.

(3) Additional iterations are needed to perform with i being replaced by $i+1$ and the calculations are resumed with Eq. (51) until the norm of correction $\Delta\bar{\boldsymbol{q}}^{(i)}_{t+\Delta t}$ is less than a prescribed error. In the present simulation examples, $\lambda = 1/4$, $\hat{\beta} = 1/2$.

7 Numerical simulation and discussions

In the rigid-flexible coupling dynamic analysis of the hub-beam system, the properties of the beam are given as follows: the mass density $\rho = 2\,766.7\,\mathrm{kg/m^3}$, the modulus of elasticity $E = 68.952\,\mathrm{GPa}$, the cross-section area $A = 80\,\mathrm{mm^2}$, and the moment of inertia $I = 1.066\,67\,\mathrm{cm^4}$.

In order to check the accuracy and the convergence of the modeling method proposed in this study, the results of the present model are compared with those obtained by commercial programs (ANSYS, ADAMS), in which straight beam elements are used to discrete curved beams.

7.1 Validation of the present modeling method

To guarantee the accuracy, the results of commercial programs are derived using sufficient number of straight beam elements to approximate the curved beam. The natural frequencies results for the stationary curved beam obtained by using the proposed modeling method are compared with those obtained by ANSYS. Four groups of dimensions for the curved beam are employed, which are represented by the following curvature radius and subtended angle: $R = 6$, $\alpha = 30°$; $R = 6$, $\alpha = 60°$; $R = 10$, $\alpha = 30°$; and $R = 10$, $\alpha = 60°$, respectively. Table 1 shows the lowest seven

natural frequencies of the stationary curved beam with the cantilevered-free boundary condition. It clearly shows that the results obtained by the present modeling method are in good agreement with those obtained from commercial program ANSYS, therefore the results in Table 1 verify the correctness of the present geometric nonlinear model by using curved beam element.

Table 1 Comparisons of natural frequencies for stationary beam (unit: Hz)

f	$R=6, \alpha=30^\circ$			$R=6, \alpha=60^\circ$			$R=10, \alpha=30^\circ$			$R=10, \alpha=60^\circ$		
	Present	ANSYS	Error/%	Present	ANSYS	Error/%	Present	ANSYS	Error/%	Present	ANSYS	Error/%
1	3.286 0	3.286 5	−0.015 2	0.851 39	0.845 86	0.649 5	1.183 1	1.183 1	0	0.305 6	0.300 8	1.570 7
2	19.849	19.862	−0.065 5	4.602 6	4.645 7	−0.936 4	7.150 2	7.151 4	−0.016 8	1.656 4	1.652	0.265 6
3	56.546	56.615	−0.122 0	13.714	13.875	−1.174	20.389	20.389	0	4.937 4	4.934 3	0.0628
4	111.34	111.51	−0.152 7	27.459	27.758	−1.088 9	40.208	40.172	0.089 5	9.882 4	9.872 6	0.0992
5	184.50	184.64	−0.075 9	45.953	46.294	−0.742 1	66.772	66.555	0.325	16.510	16.467	0.2604
6	276.17	275.84	0.119 5	69.550	69.468	0.117 9	100.26	99.518	0.74	24.860	24.715	0.583 3
7	385.07	383.6	0.381 8	99.315	97.264	2.065 1	140.85	139.04	1.285	35.035	34.612	1.207 4

Secondly, the straight beam finite element approximate model of the curved beam established by ANSYS are input into the ADAMS software for verification of the dynamic results. The radius and the rotary inertia of the hub are given by $R_h = 0.05\,\mathrm{m}$ and $J_h = 0.3\,\mathrm{kg}\cdot\mathrm{m}^2$, respectively. The length of the beams are equal to $5\pi/3\,\mathrm{m}$, and the corresponding subtended angle is $\alpha = 30^\circ$ and $\alpha = 60^\circ$, respectively. The following torque drives the hub in the numerical analysis

$$T = 10\sin(\omega_0 t)\,\mathrm{N}\cdot\mathrm{m}, \qquad 0 \le t \le 2\,\mathrm{s}, \tag{54}$$

where $\omega_0 = 2\pi\,\mathrm{rad}\cdot\mathrm{s}^{-1}$.

The dynamic results of the present model are compared with those of the commercial program ADAMS/Flex. The time histories of the tip longitudinal and tranverse deformations of the curved beam for $\alpha = 60^\circ$ are shown in Figs. 3 and 4, respectively. It can be seen in Fig. 3 that the longitudinal deformation results obtained by ADAMS are in good agreement with those obtained by the present model, and two results for the transverse deformation shown in Fig. 4 also coincide very well, which further verify the correctness of the present model.

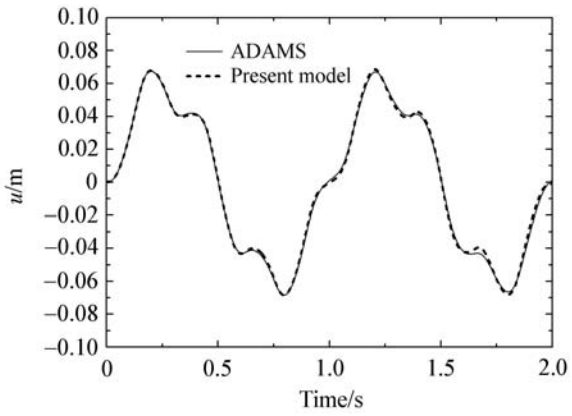

Fig. 3 The tip longitudinal deformation of the curved beam

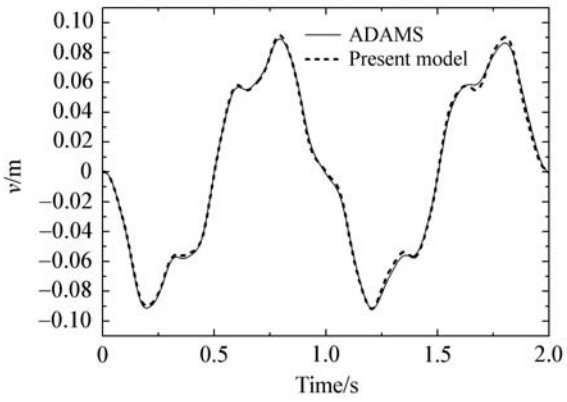

Fig. 4 The tip transverse deformation of the curved beam

7.2 Convergence rate and efficiency of the present modeling method

The convergence of the hub angular velocities obtained from the present model and the ADAMS program for $\alpha = 30^\circ$ are shown in Figs. 5 and 6, respectively. It can be seen in Fig. 5, convergence can be achieved just using at most 4 finite elements, however, at least 15 finite elements are needed to converge for the ADAMS program in Fig. 6. Therefore, the results in Figs. 5 and 6 verify that the proposed curved beam element possesses better convergence characteristic compared to the ADAMS software.

Furthermore, as can be seen in Table 2, although with the same length of 30° curved beam, for a curved beam with a subtended angle of 60°, 8 elements and 20 elements are needed to achieve convergence in the present model and in the ADAMS program, respectively. Therefore, it is concluded that for the case of the same length of the curved beam, the curved beam with larger curvature needs more elements to converge.

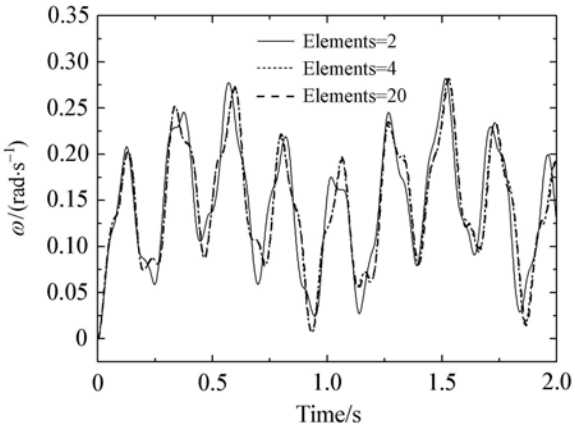

Fig. 5 Results obtained by the present model

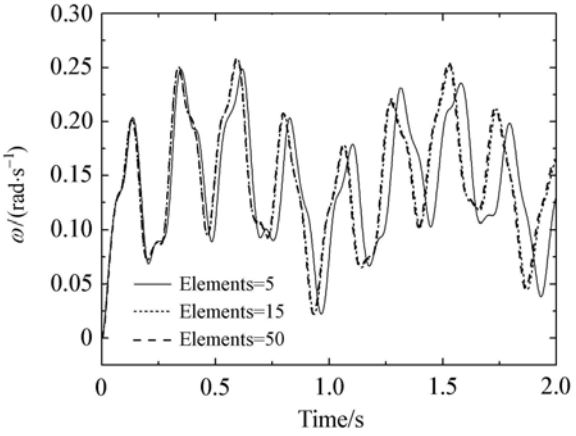

Fig. 6 Results obtained by the ADAMS software

Table 2 Comparison of the time cost and the number of beam elements needed for convergence

α	Time cost/s		Element number	
	Present model	ADAMS	Present model	ADAMS
30°	6	70	4	15
60°	12	80	8	20

In the present study, Newmark time integration scheme which are usually used for the problem of structural dynamics associated with the Newton–Raphson iteration is introduced to solve the rigid-flexible coupling problem. It is worth notice that the present numerical method is unconditionally stable for $\lambda = 1/4$, $\hat{\beta} = 1/2$ and not too small time step can be chosen to guarantee necessary accuracy. Since the mass, stiffness and internal forces matrices are functions of the system generalized coordinate, the integration process can not be completed directly by the Newmark method, which must be used in conjunction with the Newton–Raphson iteration.

Table 2 compares the time cost of the present model and the ADAMS software for simulating the dynamic model with time step 0.001 s and end time 2s. It can be seen that, for the present model, 6 seconds and 12 seconds are time cost for simulating the curved beam with 30° and 60° subtended angle, respectively, nevertheless, for the ADAMS program, the corresponding simulation time for $\alpha = 30°$ and $\alpha = 60°$ are 70 s and 80 s, respectively. It is shown that computational efficiency of the present formulation is improved significantly compared with the ADAMS software.

7.3 Example of the curved beam pendulum

As shown in Fig. 7, a curved beam pendulum under the effect of gravitational force is connected to the ground by a revolute joint. The radius of the hub is $R_h = 0$ and the moment of inertia $J_0 = 0$. To investigate the effect of geometric nonlinearity and beam shallowness, the lengths of the axis line of all the beams are $5\pi/3$ m, and the subtended angles are 60°, 30° and 20°, respectively.

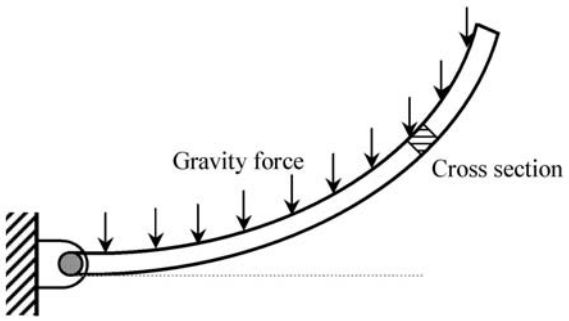

Fig. 7 The curved beam pendulum

The cross-section area is given by $A = 4\,\text{cm}^2$, and the moment of inertia is given by $I = 4/3\,\text{cm}^4$. The pendulum is released at the horizontal position with the initial conditions that $\theta = 0$, $\boldsymbol{p} = \boldsymbol{0}$, $\dot{\boldsymbol{p}} = \boldsymbol{0}$. All the deformations results are relative to the hub body-fixed frame $\boldsymbol{e}_b$.

7.3.1 Effect of the geometric nonlinearity

Figures 8 and 9 show the dynamic response of the linear and nonlinear formulation of the curved beam with a subtended angle of 20°. At the initial phase between 0 s–0.7 s, no matter it is the longitudinal or the transverse deformation, the linear and nonlinear results totally coincide. The reason is that, under the inertia force arising from the rotating motion, the original curved configuration of the curved beam tends to extend to straight configuration. During this process, the deformation is so small that the nonlinear effect is not easily excited. As the angular velocity of the pendulum increases during the period of 0.7 s–1.6 s, the nonlinear results still posses the same vibration frequency and amplitude as before, however, for the solutions of the linear formulation, vibration frequency change suddenly and the amplitude

of the deformation became large which is about three times larger than the nonlinear results, so that the linear model can not explain the dynamic stiffening phenomenon. It can be shown that when the pendulum moves near the horizontal position during the period of 1.6 s–2.5 s, the differences between the linear and nonlinear results nearly vanish, which indicate that the nonlinear effect is excited only at the position with large inertial force. Figures 10 and 11 show the longitudinal and transverse deformation of the curved beam with a subtended angle of 60°. The dynamic performance of the linear and the nonlinear model is similar to that of 20°, except that the phenomenon of the dynamic stiffening is more obvious at the plumb position.

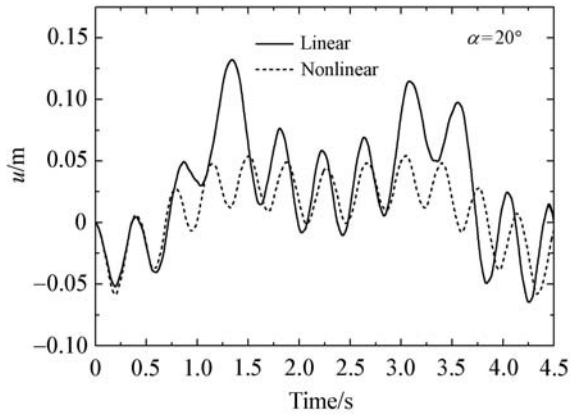

Fig. 8 The tip longitudinal deformation of the curved beam

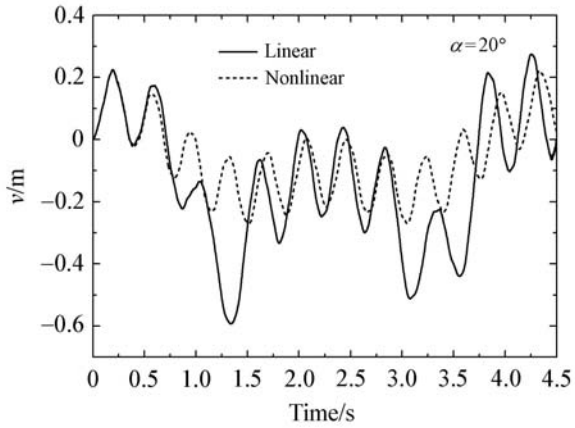

Fig. 9 The tip transverse deformation of the curved beam

7.3.2 Effect of the shallowness of the curved beam

Generally speaking, curved beams (arches) have, based on curvature, been classified as [19]: shallow arch (subtended angle < 40°) and deep arch (40° < subtended angle < 180°). All the results below are obtained by nonlinear formulation.

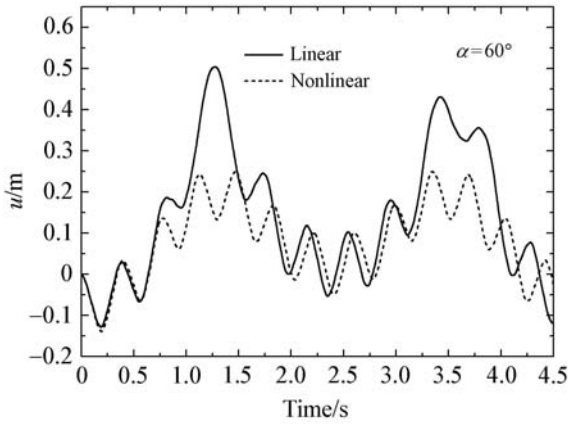

Fig. 10 The tip longitudinal deformation of the curved beam

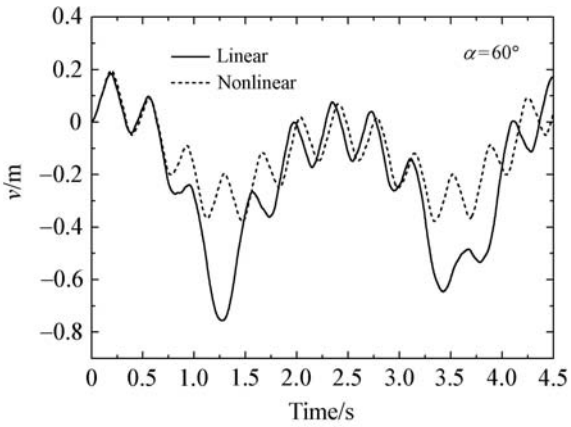

Fig. 11 The tip transverse deformation of the curved beam

Figure 12 shows the longitudinal deformation of the beam with different subtended angles. It can be seen that the deepest beam (with subtended angle of 60°) experiences the largest amplitude oscillations, and the beam with subtended angle of 20° experiences least amplitude of vibrations, similarly, the results for the transverse deformation are the same, as shown in Fig. 13. In particular, the longitudinal deformation for the cases of 60° subtended angle is approximately 2 times larger than that of 30° subtended angle, and 5 times larger than that of 20° subtended angle. Furthermore, as shown in Figs. 12 and 13, the vibration frequencies for the three cases of subtended angle are nearly identical at the beginning phase of motion, however, when the pendulum approaches the plumb position, the vibration frequency of the deepest beam becomes smaller than that of the shallow beams. Therefore, the subtended angle also influences the overall motion of the pendulum. It can be seen that the deepest beam obviously experiences the largest angle rotation and angular velocity in Figs. 14 and 15, respectively. It can be summarized that the deepest curved beam exhibits both the largest amplification elastic deformation and the largest angular rotation, but the least vibration frequency.

Particularly, as shown in Figs. 12 and 13, although the length for the straight and curved beams is the same, the dynamic results are entirely different. For the curved beam, there are two wave crests for longitudinal deformation and two wave troughs for transverse deformation, however, for the straight beam, there is only one wave trough for the transverse deformation. Furthuremore, the logitudinal deformation of the straight beam in Fig. 12 is negligibly small, on the contrary, the logitudinal deformation of curved beam are approximately 1%–5% of the beam length at two troughs.

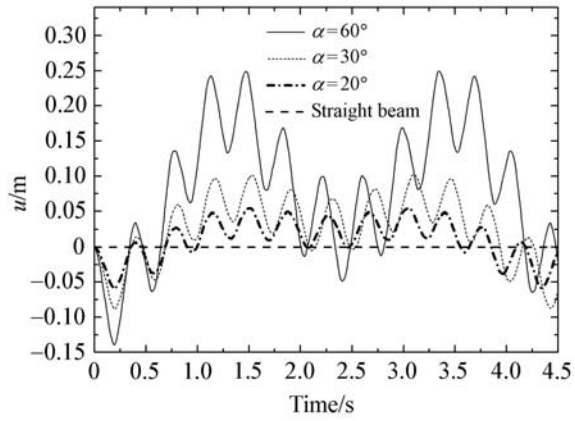

Fig. 12 The tip longitudinal deformation

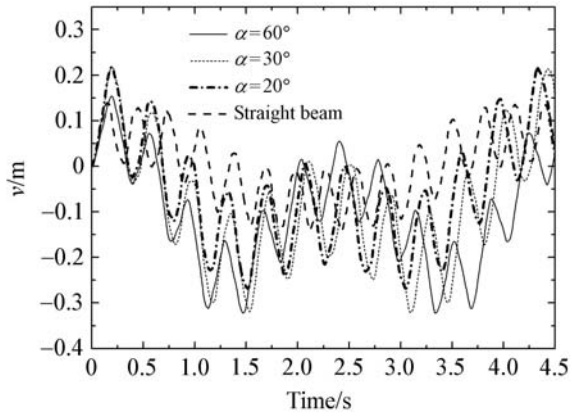

Fig. 13 The tip longitudinal deformation

8 Conclusions

Instead of using the previously-used straight beam finite element to approximate the curved beam, a curvilinear coordinate is employed to describe the deformations, and a curved beam finite element is, based on the isoparametric formulation, proposed to model the curved beam. The convergence and efficiency of the curved beam elements is verified by numerical examples. It is shown that for the approximate formulation using straight beam elements, two times the number of elements is needed to obtain accurate results compared with the present formulation using curved beam elements. Newmark and Newton–Raphson iteration methods are used for solving the differential equations of the rigid-flexible coupling system. Comparison of the present numerical method with the ADAMS program verifies the efficiency of the present method, which can be extended to solve rigid-flexible coupling problems of complicated mechanical systems.

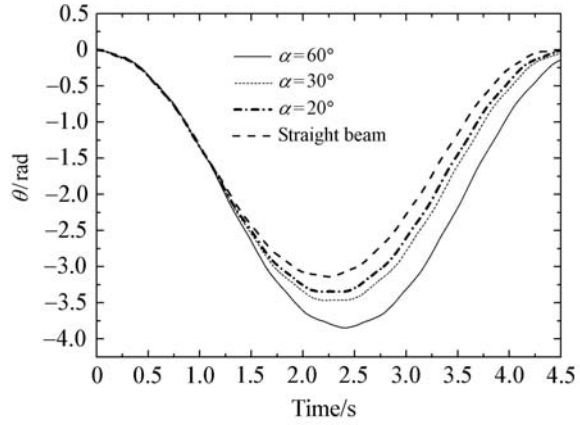

Fig. 14 The rotation angle of the rigid hub

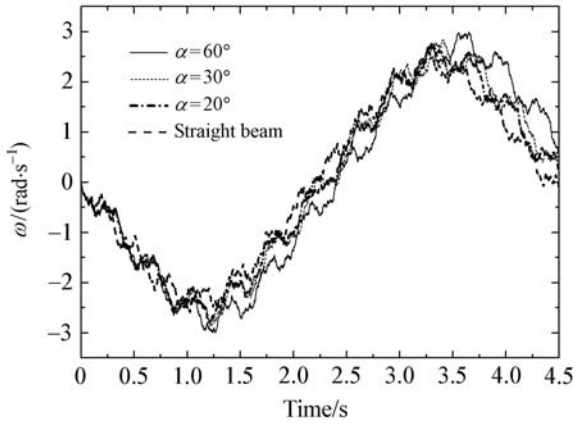

Fig. 15 The angular velocity of the rigid hub

The geometrically nonlinear effect of the straight and curved beams is analyzed. It is shown that for curved beams, the transverse and longitudinal vibration frequencies obtained by geometric nonlinear formulation are higher than those obtained by the linear formulation. In addition, the longitudinal deformation of the curved beam is so large that should be paid attention in engineering practice. It is observed that for different curved beams with the same lengths, the deepest curved beam exhibits both the largest amplification elastic deformation and the largest angular rotation, but the least vibration frequency.

References

1 Liu, J.Y., Hong, J.Z.: Geometric stiffening effect on rigid-flexible coupling dynamics of an elastic beam. J. Sound Vib. **278**, 1147–1162 (2004)

2 Yang, H.: Study on dynamic modeling theory and experiments for rigid-flexible coupling systems. [Ph.D. Thesis]. Shanghai: Shanghai Jiao Tong University (2002) (in Chinese)

3 Shabana, A.A., Mikkola, A.M.: Use of the finite element absolute nodal coordinate formulation in modeling slope discontinuity. J. Mech. Des. **125**(2), 342–350 (2003)

4 Liu, J.Y., Hong, J.Z., Cui, L.: An exact nonlinear hybrid-coordinate formulation for flexible multibody systems. Acta Mech. Sin. **23**, 699–706 (2007)

5 Liu, J.Y., Li, B., Lu, H.: Rigid flexible coupling dynamics of curvic beam considering thermal strain. Acta Mechanica Solida Sinica **28**(1), 30–35 (2007) (in Chinese)

6 Liu, Z.Y.: Study on modeling theory and simulation technique for rigid-flexible coupling system dynamics. [Ph.D. Thesis]. Shanghai: Shanghai Jiao Tong University (2008) (in Chinese)

7 Zhang, H.G., He, B.Y., Wang, S.X., et al.: Dynamic Model of flexible spatial camber beam with uncertainty parameters. Journal of Tianjin University **36**(1), 47–50 (2006) (in Chinese)

8 Sugiyama, H., Koyama, H., Yamashita, H.: Gradient deficient curved beam element using the absolute nodal coordinate formulation. ASME J. Comput. Nonlinear Dyn. **5**(2), 021001-1-021001-8 (2010)

9 Ganapathi, M., Patel, B.P., Saravanan, J.: Shear flexible curved spline beam element for static analysis. Finite Elem. Anal. Des. **32**, 181–202 (1999)

10 Raveendranath, P., Singh, G., Pradhan, B.: Free vibration of arches using a curved beam element based on a coupled polynomial displacement field. Comput. Struct. **78**, 583–590 (2000)

11 Raveendranath, P., Singh, G., Rao, G.V.: A three-noded shear-flexible curved beam element based on coupled displacement field interpolations. Int. J. Numer. Meth. Eng. **51**, 85–101 (2001)

12 Friedman, Z., Kosmatka, J.B.: An accurate two-node finite element for shear deformable curved beams. Int. J. Numer. Meth. Eng. **41**, 473–498 (1998)

13 Wu, J.S., Chiang, L.K.: Free vibration analysis of arches using curved beam elements. Int. J. Numer. Meth. Eng. **58**, 1907–1936 (2003)

14 Wu, J.S., Chiang, L.K.: Free vibration of a circularly curved Timoshenko beam normal to its initial plane using finite curved beam elements. Comput. Struct. **82**, 2525–2540 (2004)

15 Saffari, H., Tabatabaei, R., Mansouri, S.H.: Vibration analysis of circular arch element using curvature. Shock and Vibration. **15**, 481–492 (2008)

16 Yang, S.Y., Sin, H.C.: Curved-based beam elements for the analysis of Timoshenko and shear-deformation curved beams. J. Sound Vib. **187**(4), 569–584 (1995)

17 Leung, A.Y.T., Zhu, B.: Fourier p-elements for curved beam vibrations. Thin-Walled Structures **42**, 39–57 (2004)

18 Kim, J.G., Park, Y.K.: Hybrid-mixed curved beam elements with increased degrees of freedom for static and vibration analyses. Int. J. Numer. Meth. Eng. **68**(6), 690–706 (2006)

19 Park, J.H., Kim, J.H.: Dynamic analysis of rotating curved beam with tip mass. J. Sound Vib. **228**(5), 1017–1034 (1999)

20 Heppler, G.R., Hansen, J.S.: A mindlin element for thick and deep shells. Comput. Methods Appl. Mech. **54**(1), 21–47 (1986)